Article

Dual Functionalized Freestanding TiO₂ Nanotube Arrays Coated with Ag Nanoparticles and Carbon Materials for Dye-Sensitized Solar Cells

Ho-Sub Kim [1,†], Myeung-Hwan Chun [1,†], Jung Sang Suh [1], Bong-Hyun Jun [2,*] and Won-Yeop Rho [1,2,*]

[1] Department of Chemistry, Seoul National University, Seoul 151-747, Korea; hosub@snu.ac.kr (H.-S.K.); hwanmc@hanmail.net (M.-H.C.); jssuh@snu.ac.kr (J.S.S.)
[2] Department of Bioscience and Biotechnology, Konkuk University, Seoul 143-701, Korea
* Correspondence: bjun@konkuk.ac.kr (B.-H.J.); rho7272@gmail.com (W.-Y.R.); Tel.: +82-2-450-0521
† These authors contributed equally to this work.

Abstract: Highly ordered, freestanding TiO₂ nanotube arrays (TiO₂ NTAs) were prepared using an electrochemical method. The barrier layer was etched to open the bottom of each array, aptly named "open-ended TiO₂ NTAs". These arrays were coated with silver nanoparticles (Ag NPs) and/or carbon materials to enhance electron generation and transport. The energy conversion efficiency of the resulting dye-sensitized solar cells (DSSCs) with open-ended freestanding TiO₂ NTAs, when coated with Ag NPs, increased from 5.32% to 6.14% (by 15%) due to plasmonic interactions. Meanwhile, coating the open-ended freestanding TiO₂ NTAs with carbon materials increased the energy conversion efficiency from 5.32% to 6.07% (by 14%), due to π-π conjugation. When the Ag NPs and carbon materials were simultaneously applied to the open-ended freestanding TiO₂ NTAs, the energy conversion efficiency increased from 5.32% to 6.91%—an enhancement of 30%, due to the additive effects of plasmonics and π-π conjugation.

Keywords: dye-sensitized solar cells; carbon materials; Ag nanoparticles; freestanding TiO₂ nanotube arrays

1. Introduction

Since the initial development of dye-sensitized solar cells (DSSCs) in 1991 by the Grätzel group [1], global research has continued due to their low cost, ease of fabrication, and high power conversion efficiency [2,3]. Titanium dioxide nanoparticles (TiO₂ NPs) are typically used as the photoanode in DSSCs because they have a desirable direct band gap (3.2 eV) and a large surface area for adsorbing dyes; both help to generate electrons [4–7]. However, TiO₂ NPs are randomly networked, and the countless grain boundaries within them lead to material defects and charge recombinations that inhibit smooth electron transport [8–10].

In recent years, TiO₂ nanotube arrays (NTAs) have been explored as an alternative to TiO₂ NPs [11–13]. The TiO₂ NTAs can be fabricated using an electrochemical method (i.e., anodization) [11,14], and their well-ordered, vertically aligned tubular structures serve as direct electron pathways; this enhances not only electron transport, but also charge separation [15,16]. However, despite their merits, the barrier layer on the bottom of the TiO₂ NTAs may impede charge transfer and electrolyte diffusion. To overcome this problem, we recently removed the bottom layer of TiO₂ NTAs using argon ion (Ar⁺) milling, which resulted in improved electron transport and improved electrolyte diffusion [17].

There have been an increasing number of studies that add carbon to TiO_2 NTAs in order to improve the charge separation and transfer of electrons; this is due to carbon's superior electrical properties by π-π conjugation [18–20]. Many researchers have explored the application of carbon materials in solar cell technologies. Carbon 60 (C_{60} or "fullerene") and carbon nanotubes (CNTs) are well known for their roles as electron acceptors and charge separators in organic solar cells [21,22]. When incorporated in organic solar cells, CNTs act as exciton dissociation sites and hopping centers for hole transport [23], and in DSSCs, graphene mixed with TiO_2 NPs plays a role in promoting charge separation and movement [24]. As mentioned, TiO_2 NTAs were developed as alternatives to TiO_2 NPs. While it is not simple to blend carbon materials with TiO_2 NTAs, we recently reported a method for enriching freestanding TiO_2 NTAs with carbon for use in DSSCs. When a small amount of carbon was deposited on TiO_2 NTAs, compared to those without carbon enrichment, the energy conversion efficiency increased by approximately 22.4% [25]. We tentatively attributed this to an improved efficiency of electron transport by the π-π conjugation introduced through carbon enrichment.

A plasmonic effect triggered by metal NPs (such as silver and gold) can be used to enhance photoabsorption in solar cells [26–28]. When incident photons pass by Ag NPs, they cause electron vibration and photo scattering of the nanoparticles, which facilitates photon control more efficiently [29]. The metal NPs were incorporated through mixing with TiO_2 sol in the DSSCs, or with precursors of the active layer in organic solar cells. However, it is difficult to insert metal NPs into the channels of TiO_2 NTAs, as the fabrication of DSSCs based on TiO_2 NTAs requires. We recently devised a simple method for the complete formation of Ag NPs in the channels of TiO_2 NTAs using ultraviolet (UV) irradiation [13,30]. These NPs helped the dyes to generate electrons, as was demonstrated by a high current density in the DSSCs.

To date, we have confirmed the separate effects of both carbon enrichment and the incorporation of Ag NPs in previous studies. However, the effects of adding both carbon and Ag NPs remain unknown. Here, we report such effects on the performance of DSSCs—in terms of enhanced electron transport and plasmonic effects—when enriching freestanding TiO_2 NTAs with one or both materials. Carbon materials were synthesized by chemical vapor deposition (CVD) and deposited on the wall of TiO_2 NTAs. The Ag NPs were formed using UV irradiation within the channels of TiO_2 NTAs.

2. Materials and Methods

2.1. Preparation of Closed- and Open-Ended TiO$_2$ NTAs

To fabricate TiO_2 NTAs, titanium foils (Alfa Aesar, 99.7% purity, 2.5 cm $\times$ 4.0 cm $\times$ 320 μm) were prepared and anodized using an electrochemical method. The electrolyte was composed of 0.8 wt % NH_4F and 2 vol % H_2O in ethylene glycol. Carbon rods served as the cathode material. A 60 V DC potential was supplied to the titanium foils at 25 °C for 2 h. Later, the anodized titanium foils were annealed in a tube furnace (at 450 °C for 1 h), and a second anodization process was then conducted on the samples (at 30 V for 10 min). After the second anodization, the sample was immersed in 10% H_2O_2 for 24 h to detach the TiO_2 NTAs from the titanium foils. Ion milling with Ar^+ bombardment was used to make open-ended tips by removing the bottom of the TiO_2 NTAs [25].

2.2. Preparation of Photoanodes for DSSCs Based on the TiO$_2$ NTAs

Fluorine-doped tin oxide (FTO) glass was washed and sonicated in ethanol and acetone to remove impurities. Titanium diisopropoxide bis(acetylacetonate) (5 wt % in *n*-butanol) was spin-coated on the clean FTO glass to form a compact TiO_2 blocking layer after annealing at 450 °C for 1 h. A TiO_2 paste (Solaronix, T/SP) was applied to the FTO glass using a doctor blade method, in order to attach the closed- or open-ended TiO_2 NTAs. Finally, the samples were annealed in a furnace at 450 °C for 30 min.

2.3. Synthesis of Ag NPs on the TiO$_2$ NTAs by UV Irradiation

The samples were placed in a 0.3 mM AgNO$_3$ aqueous solution. Ag NPs were synthesized in the channels of closed- or open-ended TiO$_2$ NTAs using a 254 nm UV lamp for 3 min.

2.4. Synthesis of Carbon Materials on the TiO$_2$ NTAs by CVD

The samples were placed in a quartz tube furnace filled with nitrogen (200 standard cubic centimeter per minute (sccm)). Hydrogen gas (30 sccm) and ethylene gas (40 sccm) were flowed into the tube furnace at 450 °C for 30 s.

2.5. Fabrication of Dye-Sensitized Solar Cells

All DSSC samples were post-treated with 10 mM TiCl$_4$ solution at 50 °C for 30 min, then annealed at 450 °C for 1 h. These steps not only enhanced the photocurrent, but also prevented the dissolution of the Ag NPs upon contacting the iodine-iodide electrolyte. Each treated sample was stained using dye molecules in ethanol at 50 °C for 8 h; here the dye molecules were 0.5 mM solutions of N719 ((Bu$_4$N)$_2$Ru(dobpyH)$_2$(NCS)$_2$, Solaronix). Following this treatment, samples were washed with ethanol to eliminate physisorbed dye molecules. To fabricate counter electrodes, chloroplatinic acid (H$_2$PtCl$_6$) in ethanol was drop-casted onto clean FTO glass and annealed in a tube furnace at 400 °C for 1 h.

The electrolyte used to separate the electrodes contained 0.7 M 1-butyl-3-methyl-imidazolium iodide (BMII), 0.03 M I$_2$, 0.1 M guanidium thiocyanate (GSCN), and 0.5 M 4-*tert*-butyl pyridine (TBP) in a mixture of acetonitrile and valeronitrile (85:15 *v/v*). A 60-μm-thick hot-melt Surlyn spacer (Solaronix) was placed between the photoanode and counter electrode; the electrolyte was injected into the space formed.

2.6. Characterization of Dye-Sensitized Solar Cells

The structures of TiO$_2$ NTAs on FTO glass were confirmed using a field emission scanning electron microscope (FE-SEM, JSM-6330F, JEOL Inc., Tokyo, Japan) The existence of Ag NPs in the channels of TiO$_2$ NTAs was verified by the high-angle annular dark-field (HAADF) imaging technique using a scanning transmission electron microscope (TEM, JEM-2200FS, JEOL Inc., Tokyo, Japan). Raman spectra were measured using a Raman spectrometer (LabRAM HV Evolution spectrometer, HORIBA, Tokyo, Japan). The ultraviolet-visible (UV-Vis) spectra were recorded using a UV-Vis spectrophotometer (NEOSYS-2000, SCINCO, Seoul, Korea). Current density-voltage measurements were carried out using an electrometer (Keithley 2400) and a solar simulator (1 kW Xenon with AM 1.5 filter, PEC-L01, Peccel Technologies, Kanagawa, Japan). Electrochemical impedance spectroscopy (EIS) data were collected using a potentiostat (Solartron 1287) equipped with a frequency response analyzer (Solartron 1260) between 10^{-2} and 10^6 Hz under AM 1.5 light illumination, and analyzed using Z-View software (Solartron Analytical). The applied bias voltage and AC amplitude were set at the open circuit voltage (V_{oc}) of the DSSCs and at 10 mV.

3. Results and Discussion

The fabrication of DSSCs based on freestanding TiO$_2$ NTAs is shown in Figure 1. The bottom layer was present in the closed-ended freestanding TiO$_2$ NTAs, but was removed by ion milling in the open-ended TiO$_2$ NTAs. The DSSCs were fabricated from both the open- and closed-ended freestanding TiO$_2$ NTAs to compare energy conversion efficiencies. In both cases, the freestanding TiO$_2$ NTAs were attached to the FTO glass with TiO$_2$ paste, and Ag NPs were synthesized using UV irradiation (Figure 1a). Carbon materials were synthesized using CVD (Figure 1b). By using the UV irradiation and CVD, Ag NPs and carbon materials were deposited in the channel of highly ordered TiO$_2$ NTAs without any distortion. The dye (N719) was adsorbed onto both types of freestanding TiO$_2$ NTAs (Figure 1c). Finally, DSSCs were fabricated by assembling the working electrode (freestanding TiO$_2$ NTAs on FTO glass) and the counter electrode (Pt on FTO glass), as shown in Figure 1d.

FE-SEM images of TiO_2 NTAs are shown in Figure 2. The top view (Figure 2a) shows a pore size of approximately 100 nm after having applied the electrochemical method. The bottom of the TiO_2 NTAs before ion milling ("closed-ended TiO_2 NTAs") is shown in Figure 2b, with a total bottom pore size of approximately 100 nm (including that of the wall thickness). However, when the bottom was removed by ion milling to produce the "open-ended TiO_2 NTAs" (Figure 2c), the bottom pore was reduced to 30 nm in size, while the wall thickness was approximately 35 nm. An HAADF image of Ag NPs in the channels of TiO_2 NTAs is shown in Figure 2d, and the diameter of Ag NPs was approximately 30 nm. This allowed the Ag NPs to be successfully immobilized inside the channel of TiO_2 NTAs by UV irradiation, and the resulting plasmonic interactions may have affected all the surface areas. A side view of TiO_2 NTAs attached to the FTO glass by TiO_2 paste after being sintered at 450 °C is shown in Figure 2e. The main role of the TiO_2 paste is to connect the TiO_2 NTAs with the FTO glass surface. The thickness of the TiO_2 film layer was 3 μm, and the length of the TiO_2 NTAs was approximately 18 μm.
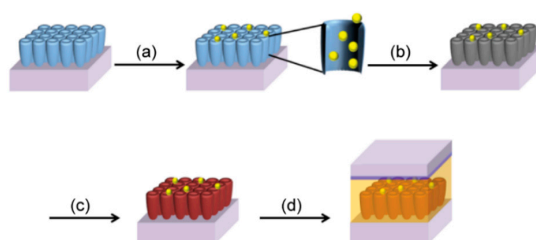

Figure 1. Overall scheme of the fabrication of dye-sensitized solar cells (DSSCs), based on freestanding TiO_2 nanotube arrays (TiO_2 NTAs) coated with silver nanoparticles (Ag NPs) and carbon materials. (**a**) Synthesis of Ag NPs in the channel of TiO_2 NTAs, (**b**) deposition of carbon materials, (**c**) dye adsorption, and (**d**) fabrication of the DSSC.
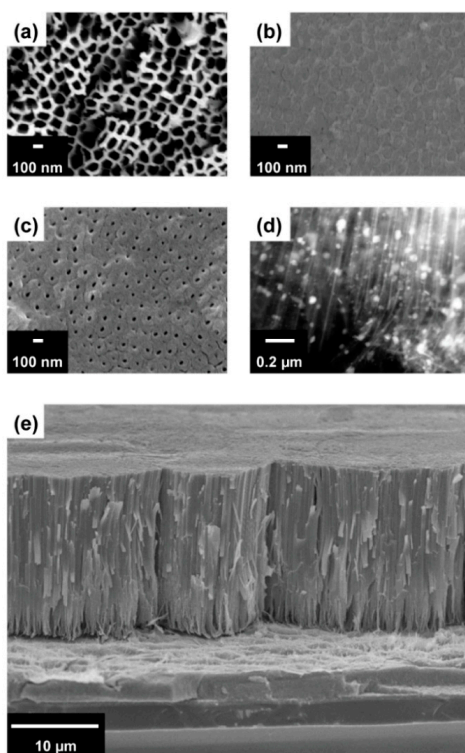

Figure 2. Field emission scanning electron microscope (FE-SEM) images of TiO_2 NTAs: (**a**) top view, (**b**) bottom view, (**c**) bottom view after ion milling, (**d**) high-angle annular dark-field (HAADF) image of Ag NPs in the channel of TiO_2 NTAs, and (**e**) side view of TiO_2 NTAs on fluorine-doped tin oxide (FTO) glass.

Carbon materials on the TiO_2 NTAs were synthesized by CVD, and Figure 3 shows their structure as confirmed by Raman spectroscopy (TEM images of TiO_2 NTAs were shown in Figure S1). In a previous publication, we reported the optimization of TiO_2 NTAs for DSSCs using carbon materials [25]. The B_{1g} (397 cm^{-1}), A_{1g} (518 cm^{-1}), and E_g (641 cm^{-1}) peaks indicated that the TiO_2 NTAs were in the form of anatase TiO_2, as shown in Figure 3a [31]. When carbon materials were synthesized on the TiO_2 NTAs using CVD, the G band at 1600 cm^{-1} represented graphite, while the D band at 1384 cm^{-1} was due to the disorderly network of sp^2 and sp^3 sites in the carbon materials (Figure 3b). The sp^2 sites of the carbon materials resulted in a π-π conjugation that improved the efficiency of electron transport across the TiO_2 NTAs.
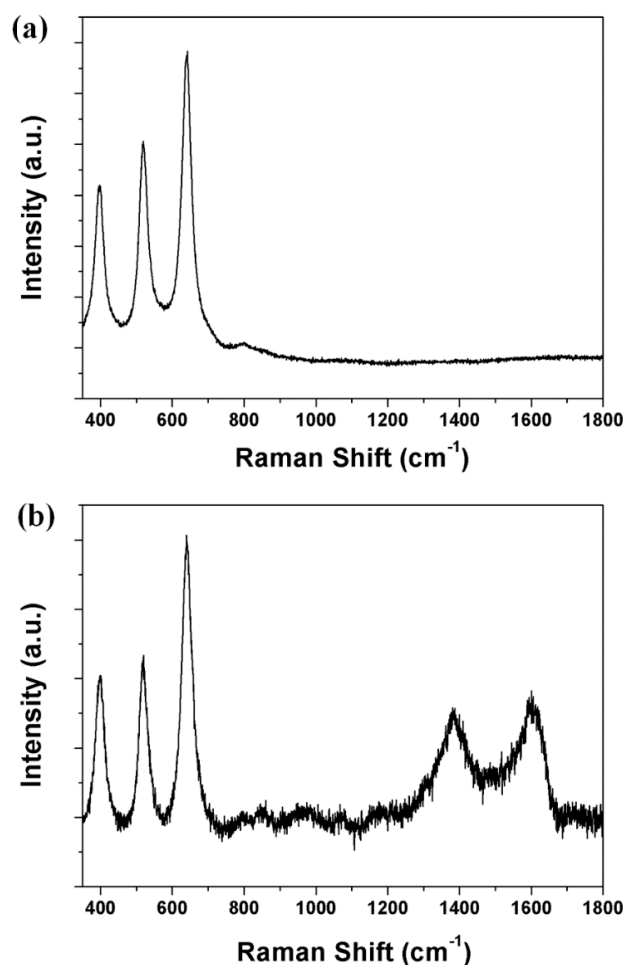

Figure 3. Raman spectra of TiO_2 NTAs: (**a**) without carbon materials, and (**b**) with carbon materials.

Ag NPs were synthesized on the TiO_2 NTAs using UV irradiation, and this was confirmed by the UV-Vis spectrum. Using the HAADF image shown in Figure 2d, the size of Ag NPs was confirmed to be approximately 30 nm. An absorption peak centered at 405 nm was also observed (Figure 4). Our previous paper reported on the optimization of TiO_2 NTAs using Ag NPs [25]. Other researchers have reported that Ag NPs with sizes of approximately 30 nm had UV-Vis absorption peaks at 420 nm. However, in this case, the Ag NPs were synthesized using UV irradiation (at 254 nm) without the addition of any stabilizing or reducing agents. As such, the Ag NPs were immobilized in the TiO_2 NTAs, which would affect absorption in the UV-Vis spectrum. The absorption band of Ag NPs is within the same range as that of the dye N719 (*cis*-diisothiocyanato-bis(2,2'-bityridyl-4,4'-dicarboxylato) ruthenium(II) bis(tetrabutylammonium), 390–530 nm), which led to enhanced electron generation from the dye by means of plasmonic interactions.
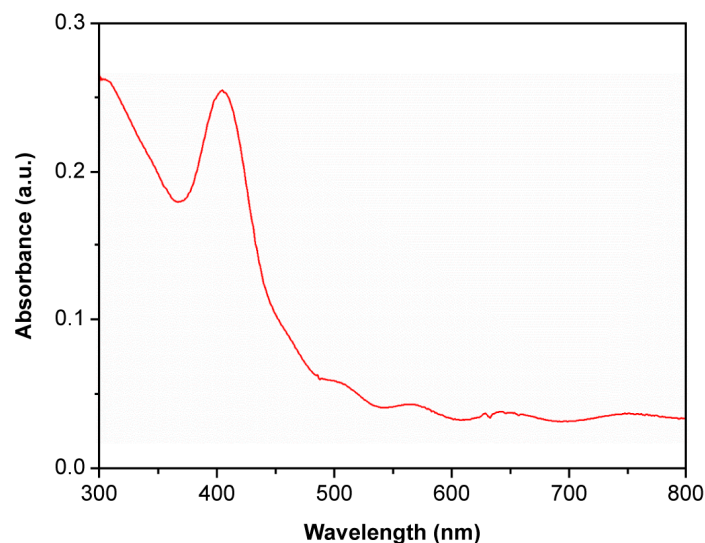
Figure 4. Ultraviolet-visible (UV-Vis) spectrum of Ag NPs on the TiO$_2$ NTAs.

The current density-voltage curves of DSSCs using closed-ended TiO$_2$ NTAs both with and without modification were measured under air-mass (AM) 1.5 sunlight, and the results are presented in Figure 5. The V_{oc}, short-circuit current density (J_{sc}), fill factor (ff), and energy conversion efficiency (η) of the DSSCs are summarized in Table 1. For the DSSCs without any treatment, the energy conversion efficiency was 4.10%, which increased to 5.73% when Ag NPs were embedded via UV irradiation (corresponding to an overall increase of 40%). When carbon materials were added to the closed-ended TiO$_2$ NTAs via CVD, the energy conversion efficiency improved to 5.69%, corresponding to a 39% increase. With both Ag NPs and carbon materials, the energy conversion efficiency further improved to 6.36%, corresponding to an overall increase of 55%. Note that when Ag NPs were treated with TiCl$_4$, the core-shell type Ag@TiO$_2$ nanoparticles were formed. Because the dye is adsorbed on Ag@TiO$_2$, the amount of dye loading may not be significantly reduced (Table 1). As previously reported, a large amount of carbon doping materials could lower the conversion efficiency by decreasing dye loading [25]. However, in this case, only a trace amount of carbon material was deposited, which did not significantly decrease the dye loading.
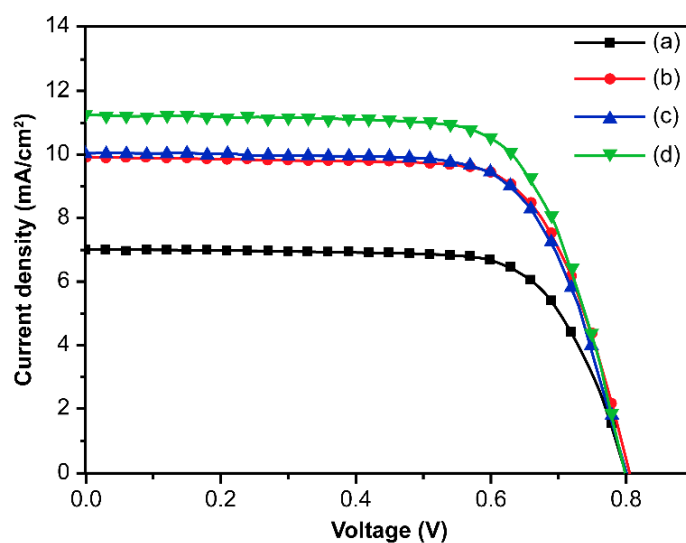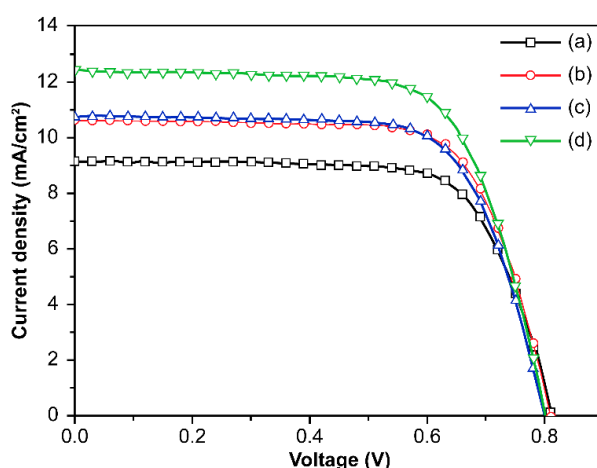

Figure 5. Current density-voltage curves of DSSCs based on: (a) unmodified closed-ended TiO$_2$ NTAs, (b) embedded Ag NPs, (c) applied carbon materials, and (d) both Ag NPs and carbon materials.

Table 1. Photovoltaic properties of dye-sensitized solar cells (DSSCs) based on closed-ended TiO_2 nanotube arrays (TiO_2 NTAs) with Ag nanoparticles (NPs) and/or carbon materials.

DSSCs Based on Closed-Ended TiO_2 NTAs Decorated	J_{sc} (mA/cm^2)	V_{oc} (V)	*ff*	η (%)	Dye Loading (nmol/cm^2)
without Ag NPs and carbon materials	7.02	0.81	0.72	4.10 ± 0.28	144
with Ag NPs	9.92	0.81	0.72	5.73 ± 0.31	142
with carbon materials	10.03	0.80	0.71	5.69 ± 0.26	139
with Ag NPs and carbon materials	11.25	0.80	0.71	6.36 ± 0.34	141

The current density-voltage curves for DSSCs based on open-ended TiO_2 NTAs with or without modification were also measured under AM 1.5 sunlight, and the results are presented in Figure 6. The V_{oc}, J_{sc}, *ff* and η values of these DSSCs are summarized in Table 2. When unmodified TiO_2 NTAs were used, DSSCs based on open-ended TiO_2 NTAs had higher energy conversion efficiency (5.32%) compared to those based on closed-ended TiO_2 NTAs (4.10%). The closed-end barrier of the TiO_2 NTA disturbs electron transport between the TiO_2 layer and the electrode [17,25].

Figure 6. Current density-voltage curves of DSSCs based on: (a) unmodified open-ended TiO_2 NTAs, (b) embedded Ag NPs, (c) applied carbon materials, and (d) both Ag NPs and carbon materials.

Table 2. Photovoltaic properties of DSSCs based on open-ended TiO_2 NTAs with Ag NPs and/or carbon materials.

DSSCs Based on Open-Ended TiO_2 NTAs Decorated	J_{sc} (mA/cm^2)	V_{oc} (V)	*ff*	η (%)	Dye Loading (nmol/cm^2)
without Ag NPs and carbon materials	9.12	0.81	0.72	5.32 ± 0.36	153
with Ag NPs	10.61	0.81	0.71	6.14 ± 0.46	151
with carbon materials	10.73	0.80	0.71	6.07 ± 0.30	147
with Ag NPs and carbon materials	12.41	0.80	0.69	6.91 ± 0.41	149

When Ag NPs were embedded in the open-ended TiO_2 NTAs, the energy conversion efficiency improved from 5.32% to 6.14%, corresponding to a 15% enhancement. In this case, electron generation in the DSSCs was enhanced by the plasmonics from the NPs, despite the slightly diminished dye loading (from 153 to 151 nmol/cm^2). When carbon materials alone were applied to TiO_2 NTAs, the energy conversion efficiency improved to 6.07% (a 14% increase). In this case, electron transport was improved due to the π-π conjugation across the small quantity of carbon materials in spite of a diminished dye load (153 to 147 nmol/cm^2, which was even less than with Ag NPs). Here carbon materials were distributed to interact with the TiO_2 and the dye, making up for the loss of dye loading in terms of the energy conversion efficiency. When Ag NPs and carbon materials were both applied to

the open-ended TiO_2 NTAs, the energy conversion efficiency improved to 6.91%, corresponding to a 30% enhancement when compared to the unmodified open-ended TiO_2 NTAs. In this case, the Ag NPs and carbon materials produced additive effects with their respective plasmonics and π-π conjugations; this was in spite of a slightly reduced dye loading of 149 nmol/cm^2. Comparing the performance parameters in Table 2, the V_{oc} and *ff* decreased with treatment; the conduction band of the TiO_2 NTAs shifted down as shown in Figure S2, which in turn affected the V_{oc} and the charge recombination through electron density suppressing the *ff*. However, the J_{sc} was increased by the plasmonic activity in conjunction with π-π, which improved the energy conversion efficiency of the DSSCs.

The DSSCs based on open-ended TiO_2 NTAs were characterized by EIS across the frequency range from 10^{-2} to 10^6 Hz, as shown in Figure 7. The applied bias voltage was set at the V_{oc} with 10 mV of AC amplitude. The data were analyzed using an equivalent circuit (Figure 7 inset), and the fit parameters are listed in Table 3. The ohmic series resistance (R_s) was due to the sheet resistance corresponding to the x-axis value where the first semicircle begins (on the left-hand side of Figure 7). The value of R_s was similar with or without Ag NPs or carbon materials, indicating that the additional deposits did not affect the sheet's resistance to FTO or the current collector. The R_1 value is given by the sum of the small semicircle, which at high frequency was assigned to the parallel combination of resistances and the capacitances at the Pt-FTO/electrolyte and the FTO/TiO_2 interfaces. The R_2 value is given by the sum of the large semicircle at low frequency (associated with the resistance) and the capacitance at the dye-adsorbed TiO_2/electrolyte interface, as well as the transport resistance. The values of R_1 without and with Ag NPs were approximately 5.58 and 5.54 Ω, respectively. However, the value of R_2 with Ag NPs (36.90 Ω) was much lower than without Ag NPs (61.12 Ω). More electrons were generated by plasmonic activities than were produced at the dye-adsorbed TiO_2/electrolyte interface. As a result, the R_2 value was reduced in the presence of Ag NPs. The value of R_1 with carbon materials (5.07 Ω) was less than for without or with Ag NPs (5.58 and 5.54 Ω, respectively), whereas the value of R_2 (36.40 Ω) was less than without Ag NPs (61.12 Ω). Electrons were better transported by π-π conjugation affected by the FTO/TiO_2 and dye-adsorbed TiO_2/electrolyte interfaces. Hence, the values of both R_1 and R_2 decreased in the presence of carbon materials. In the presence of both Ag NPs and carbon materials, the values of R_1 (4.88 Ω) and R_2 (24.55 Ω) were the lowest. In this case, more electrons were generated and better transported by a combination of plasmonics and the π-π conjugation affecting the FTO/TiO_2 and dye-adsorbed TiO_2/electrolyte interfaces. Therefore, the values of R_1 and R_2 were reduced and the parameters were determined by EIS, as shown in Table S1.
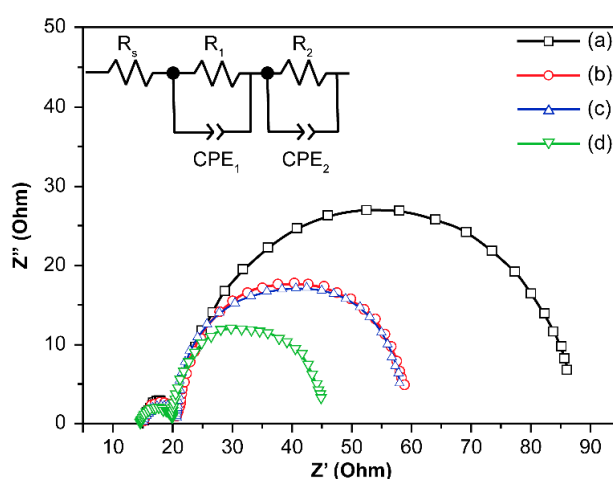

Figure 7. Electrochemical impedance spectroscopy (EIS) data of DSSCs based on: (a) unmodified open-ended TiO_2 NTAs, (b) embedded Ag NPs, (c) applied with carbon materials, and (d) with both Ag NPs and carbon materials.

Table 3. EIS fitting results for DSSCs with open-ended TiO_2 NTAs.

DSSCs Based on Open-Ended TiO_2 NTAs Decorated	R_s (Ω)	R_1 (Ω)	CPE_1 (F)	R_2 (Ω)	CPE_2 (F)
without Ag NPs and carbon materials	15.50	5.58	6.91×10^{-6}	61.12	1.99×10^{-3}
with Ag NPs	15.52	5.54	8.65×10^{-6}	36.90	2.10×10^{-3}
with carbon materials	15.56	5.07	1.62×10^{-5}	36.40	2.03×10^{-3}
with Ag NPs and carbon materials	14.99	4.88	1.16×10^{-6}	24.55	2.99×10^{-3}

The incident photon-to-current efficiency (IPCE) of DSSCs based on the open-ended TiO_2 NTAs is shown in Figure 8. Plasmon is a type of quasiparticle consisting of free electrons collectively vibrating within the metal. At the interface of a metal with a negative dielectric constant and a medium with a positive dielectric constant, surface plasmon resonance (SPR) combines a spreading electromagnetic wave (from visible to near-infrared frequency) with the plasmon. This combination generates plasmon-polariton, which leads to optical absorption; a strong electric field is also generated in some parts. During SPR, the light energy accumulates on the metal nanoparticle surface, and optical control is possible in the frequency range below the optical diffraction limit. Therefore, the intensity of DSSC based on open-ended TiO_2 NTAs embedded with Ag NPs was higher than without embedded Ag NPs. This may mean that more electrons were generated by the plasmonic activities, which increased the short circuit current. The current intensity in the DSSCs based on open-ended TiO_2 NTAs with carbon materials was also higher than in those without. This may mean that electrons were better transported by π-π conjugation, which also increased the short circuit current. Moreover, the current intensity was the strongest in the presence of both Ag NPs and carbon materials. In this case, electrons were generated in large quantities and were better transported by plasmonic activities and π-π conjugation.
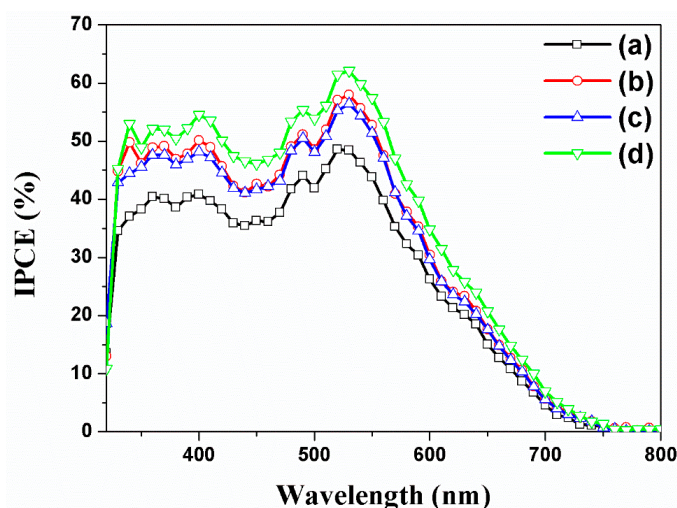

Figure 8. Incident photon-to-current efficiency (IPCE) of DSSCs based on: (a) unmodified open-ended TiO_2 NTAs, (b) embedded with Ag NPs, (c) applied with carbon materials, and (d) with both Ag NPs and carbon materials.

4. Conclusions

We deposited Ag NPs and carbon materials in the channels of closed- and open-ended TiO_2 NTAs using UV irradiation and CVD, respectively. These modifications improved the energy conversion efficiency of the corresponding DSSCs; the electron generation was enhanced by plasmonics from the Ag NPs, while the resistance of TiO_2 NTAs was suppressed via the π-π conjugation from the carbon materials. DSSCs made of freestanding TiO_2 NTAs coated with both Ag NPs and carbon materials

had the best energy conversion efficiency, due to the combination of these two factors. Comparing the open-ended and closed-ended TiO_2 NTAs (both with Ag NPs and carbon materials), the energy conversion efficiency of the DSSCs was higher for the former.

Author Contributions: H.-S. Kim, M.-H. Chun, J.S. Suh, B.-H. Jun, and W.-Y. Rho conceived and designed the experiments. H.-S. Kim and W.-Y. Rho performed the experiments. H.-S. Kim, and M.-H. Chun analyzed the data. H.-S. Kim, B.-H. Jun, and W.-Y. Rho wrote the manuscript. All authors read and approved the final manuscript.

Conflicts of Interest: The authors declare no conflict of interest.

References

1.　Oregan, B.; Grätzel, M. A low-cost, high-efficiency solar cell based on dye-sensitized colloidal TiO_2 films. *Nature* **1991**, *353*, 737–740. [CrossRef]

2.　Grätzel, M.J. Dye-sensitized solar cells. *Photochem. Photobiol. C Photochem. Rev.* **2003**, *4*, 145–153. [CrossRef]

3.　Hardin, B.E.; Snaith, H.J.; McGehee, M.D. The renaissance of dye-sensitized solar cells. *Nat. Photonics* **2012**, *6*, 162–169. [CrossRef]

4.　Sang, L.; Zhao, Y.; Burda, C. TiO_2 Nanoparticles as functional building blocks. *Chem. Rev.* **2014**, *114*, 9283–9318. [CrossRef] [PubMed]

5.　Hara, K.; Sato, T.; Katoh, R.; Furube, A.; Ohga, Y.; Shinpo, A.; Suga, S.; Sayama, K.; Sugihara, H.; Arakawa, H. Molecular design of coumarin dyes for efficient dye-sensitized solar cells. *J. Phys. Chem. B* **2003**, *107*, 597–606. [CrossRef]

6.　Galoppini, E. Linkers for anchoring sensitizers to semiconductor nanoparticles. *Coord. Chem. Rev.* **2004**, *248*, 1283–1297. [CrossRef]

7.　Nazeeruddin, M.K.; Pechy, P.; Renouard, T.; Zakeeruddin, S.M.; Humphry-Baker, R.; Comte, P.; Liska, P.; Cevey, L.; Costa, E.; Shklover, V.; et al. Engineering of efficient panchromatic sensitizers for nanocrystalline TiO_2-based solar cells. *J. Am. Chem. Soc.* **2001**, *123*, 1613–1624. [CrossRef] [PubMed]

8.　Grätzel, M. Photoelectrochemical cells. *Nature* **2001**, *414*, 338–344. [CrossRef] [PubMed]

9.　Katoh, R.; Furube, A.; Yoshihara, T.; Hara, K.; Fujihashi, G.; Takano, S.; Murata, S.; Arakawa, H.; Tachiya, M. Efficiencies of electron injection from excited N3 into nanocrystalline semiconductor (ZrO_2, TiO_2, ZnO, Nb_2O_5, SnO_2, In_2O_3) films. *J. Phys. Chem. B* **2004**, *108*, 4818–4822. [CrossRef]

10.　Du, L.; Furube, A.; Yamamoto, K.; Hara, K.; Katoh, R.; Tachiya, M. Plasmon-induced charge separation and recombination dynamics in gold–TiO_2 nanoparticle systems: Dependence on TiO_2 particle size. *J. Phys. Chem. C* **2009**, *113*, 6454–6462. [CrossRef]

11.　Mor, G.K.; Varghese, O.K.; Paulose, M.; Shankar, K.; Grimes, C.A. A review on highly ordered, vertically oriented TiO_2 nanotube arrays: Fabrication, material properties, and solar energy applications. *Sol. Energy Mater. Sol. Cells* **2006**, *90*, 2011–2075. [CrossRef]

12.　Shin, Y.; Lee, S. Self-organized regular arrays of anodic TiO_2 nanotubes. *Nano Lett.* **2008**, *8*, 3171–3173. [CrossRef] [PubMed]

13.　Rho, W.-Y.; Jeon, H.; Kim, H.-S.; Chung, W.-J.; Suh, J.S.; Jun, B.-H. Ag Nanoparticle–functionalized open-ended freestanding TiO_2 nanotube arrays with a scattering layer for improved energy conversion efficiency in dye-sensitized solar cells. *J. Nanomater.* **2016**, *6*, 117. [CrossRef] [PubMed]

14.　Ruan, C.M.; Paulose, M.; Varghese, O.K.; Mor, G.K.; Grimes, C.A. Fabrication of highly ordered TiO_2 nanotube arrays using an organic electrolyte. *J. Phys. Chem. B* **2005**, *109*, 15754–15759. [CrossRef] [PubMed]

15.　Martinson, A.B.; Hamann, T.W.; Pellin, M.J.; Hupp, J.T. New architectures for dye-sensitized solar cells. *Chemistry* **2008**, *14*, 4458–4467. [CrossRef] [PubMed]

16.　Chen, Q.W.; Xu, D.S. Large-scale, noncurling, and free-standing crystallized TiO_2 nanotube arrays for dye-sensitized solar cells. *J. Phys. Chem. C* **2009**, *113*, 6310–6314. [CrossRef]

17.　Rho, C.; Min, J.H.; Suh, J.S. barrier layer effect on the electron transport of the dye-sensitized solar cells based on TiO_2 nanotube arrays. *J. Phys. Chem. C* **2012**, *116*, 7213–7218. [CrossRef]

18. Zhang, H.; Lv, X.; Li, Y.; Wang, Y.; Li, J. P25-graphene composite as a high performance photocatalyst. *ACS Nano* **2010**, *4*, 380–386. [CrossRef] [PubMed]

19. Wang, W.; Bando, Y.; Zhi, C.; Fu, W.; Wang, E.; Golberg, D. Aqueous noncovalent functionalization and controlled near-surface carbon doping of multiwalled boron nitride nanotubes. *J. Am. Chem. Soc.* **2008**, *130*, 8144–8145. [CrossRef] [PubMed]

20. Guo, X.; Baumgarten, M.; Müllen, K. Designing π-conjugated polymers for organic electronics. *Prog. Polym. Sci.* **2013**, *38*, 1832–1908. [CrossRef]

21. Schulze, K.; Uhrich, C.; Schüppel, R.; Leo, K.; Pfeiffer, M.; Brier, E.; Reinold, E.; Baeuerle, P. Efficient vacuum-deposited organic solar cells based on a new low-bandgap oligothiophene and fullerene C60. *Adv. Mater.* **2006**, *18*, 2872–2875. [CrossRef]

22. Cheng, Y.-J.; Yang, S.-H.; Hsu, C.-S. Synthesis of conjugated polymers for organic solar cell applications. *Chem. Rev.* **2009**, *109*, 5868–5923. [CrossRef] [PubMed]

23. Pradhan, B.; Batabyal, S.K.; Pal, A.J. Functionalized carbon nanotubes in donor/acceptor-type photovoltaic devices. *Appl. Phys. Lett.* **2006**, *88*, 3106. [CrossRef]

24. Roy-Mayhew, J.D.; Aksay, I.A. Graphene materials and their use in dye-sensitized solar cells. *Chem. Rev.* **2014**, *114*, 6323–6348. [CrossRef] [PubMed]

25. Rho, W.-Y.; Kim, S.-H.; Kim, H.-M.; Suh, J.S.; Jun, B.-H. Carbon-doped freestanding TiO_2 nanotube arrays in dye-sensitized solar cells. *New J. Chem.* **2017**, *41*, 285–289. [CrossRef]

26. Lu, L.; Luo, Z.; Xu, T.; Yu, L. Cooperative plasmonic effect of Ag and Au nanoparticles on enhancing performance of polymer solar cells. *Nano Lett.* **2012**, *13*, 59–64. [CrossRef] [PubMed]

27. Pillai, S.; Catchpole, K.; Trupke, T.; Green, M. Surface plasmon enhanced silicon solar cells. *J. Appl. Phys.* **2007**, *101*, 093105. [CrossRef]

28. Nakayama, K.; Tanabe, K.; Atwater, H.A. Plasmonic nanoparticle enhanced light absorption in GaAs solar cells. *Appl. Phys. Lett.* **2008**, *93*, 121904. [CrossRef]

29. Bhattacharyya, D.; Sarswat, P.K.; Islam, M.; Kumar, G.; Misra, M.; Free, M.L. Geometrical modifications and tuning of optical and surface plasmon resonance behaviour of au and ag coated tio 2 nanotubular arrays. *RSC Adv.* **2015**, *5*, 70361–70370. [CrossRef]

30. Rho, W.-Y.; Kim, H.-S.; Lee, S.H.; Jung, S.; Suh, J.S.; Hahn, Y.-B.; Jun, B.-H. Front-illuminated dye-sensitized solar cells with Ag nanoparticle-functionalized freestanding TiO_2 nanotube arrays. *Chem. Phys. Lett.* **2014**, *614*, 78–81. [CrossRef]

31. Yan, J.; Wu, G.; Guan, N.; Li, L.; Li, Z.; Cao, X. Understanding the effect of surface/bulk defects on the photocatalytic activity of TiO_2: Anatase versus rutile. *Phys. Chem. Chem. Phys.* **2013**, *15*, 10978–10988. [CrossRef] [PubMed]